View Article Online / Journal Homepage / Table of Contents for this issue

PCCP

Theoretical study of hydrogen abstraction from dimethyl ether and methyl *tert*-butyl ether by hydroxyl radical†

F. Atadinç, C. Selçuki, L. Sari and V. Aviyente*

Bogaziçi University, Chemistry Department, 80815, Bebek, Istanbul, Turkey. E-mail: aviye@boun.edu.tr; Fax: +90 212 2872467; Tel: +90 212 3581540 1670

Received 31st October 2001, Accepted 23rd January 2002
First published as an Advance Article on the web 16th April 2002

Published on 16 April 2002. Downloaded by Pennsylvania State University on 17/09/2016 11:27:06.

MP2/6-31G**//MP2/6-31G**, PMP2/6-31G**//MP2/6-31G**, MP4/6-311G(3df,2p)//MP2/6-31G**, PMP4/6-311G(3df,2p)//MP2/6-31G** and CCSD(T)/6-311++G**//MP2/6-31G** calculations have been used to investigate the H-abstraction reaction from CH_3OCH_3 (DME) whereas MP2/6-31G**//MP2/6-31G** and PMP2/6-31G**//MP2/6-31G** levels have been used to model the H-abstraction reaction from $(CH_3)_3COCH_3$ (MTBE) by $^{\bullet}OH$. The methodology used has been proved to be adequate to reproduce the experimental geometrical parameters for the reactants and the C–H bond energies. The reaction rate constants for DME, calculated using the transition state theory reproduce the reported experimental results. The fact that H-abstraction is favored from the methoxy group of MTBE in comparison to the *tert*-butyl group has also been reproduced.

Introduction

Ethers are used as industrial solvents and additives to unleaded gasoline to increase the octane rating. They are released to the atmosphere through evaporation and are degraded in the troposphere *via* their reactions with hydroxyl radicals.[1] Dimethyl ether (DME) has been proposed as an alternative diesel fuel.[2,3] Since the emission of DME to the atmosphere may be harmful to the environment, the atmospheric chemistry of DME is very important due to the fact that the rate of the reaction with hydroxyl radical dictates the atmospheric lifetime of DME.

Methyl *tert*-butyl ether (MTBE) is used as a motor fuel additive in gasoline to reduce CO emissions.[4] MTBE has a high octane number and is used to boost the octane number of gasoline. Both ethers are adopted as important components in reformulated gasolines developed by major petroleum companies. On the other hand, the U.S. Environmental Protection Agency (EPA) has recently classified MTBE as a possible cancer-causing agent.[5] Toxicity[6] and carcinogenicity studies[7,8] have linked MTBE to actual human illness. MTBE is soluble in water and moves in soils, rivers, lakes and underground water supplies. MTBE is known to be volatile and readily undergoes UV-initiated decomposition in the atmosphere.[9]

Following the release of such volatile organic compounds, the main atmospheric fate of ethers is expected to be the reaction with $^{\bullet}OH$ which is the important step in the oxidation of ethers in the atmosphere and in the combustion systems. Since saturated organic compounds containing hydrogen atoms are expected to be oxidized by $^{\bullet}OH$,[9] the atmospheric lifetime is determined primarily by the reaction rate of these molecules against $^{\bullet}OH$. Thus, the study of the reactivity against $^{\bullet}OH$ is crucial for the evaluation of the atmospheric lifetime of these molecules.

To understand the atmospheric impact on the reactivity of automobile emissions in the troposphere, the mechanism of their oxidation and the kinetic data on their reactivity towards $^{\bullet}OH$ must be investigated. Accurate kinetic data for the rates of reaction of these species with $^{\bullet}OH$ are required to model their chemistry in the atmosphere from industrial releases and in combustion processes. To degrade organic pollutants in surface and ground-water supplies by $^{\bullet}OH$ is also known as an attractive alternative method.[10]

Recently, the gas phase structures and properties of MTBE have been calculated using a variety of *ab initio* methods. Results have been discussed in light of known experimental and environmental phenomena.[11] The reactions between oxygen-containing organic pollutants (H_2CO, H_3COH, H_3COCH_3, H_2CCH_2O) and OH have been investigated at different levels of theory using either the 6-31G* or the 6-311G** basis sets. The results have shown that satisfactory agreement with the available experimental data can be obtained using the QCISD method with the 6-311G** basis set. Reasonable results are also obtained at the MP2/6-311G** level. The geometrical parameters computed with the 6-31G* basis set agree well with those provided by the 6-311G** basis. In this study, the inadequacy of the DFT approach (B3LYP, B3PW91, BLYP) has also been pointed out.[12]

In the present study, the potential energy surface of the hydrogen abstraction by $^{\bullet}OH$ from DME and MTBE has been modeled at the MP2/6-31G** level. However, the kinetic parameters for the hydrogen abstraction from DME have been calculated at MP2/6-31G**//MP2/6-31G**, PMP2/6-31G**//MP2/6-31G**, MP4/6-311G(3df,2p)//MP2/6-31G**, PMP4/6-311G(3df,2p)//MP2/6-31G** and CCSD(T)/6-311++G**//MP2/6-31G** levels, whereas those related to MTBE have been calculated at the MP2/6-31G**//MP2/6-31G** and PMP2/6-31G**//MP2/6-31G** levels.

† Electronic supplementary information (ESI) available: optimized structural parameters, energies, zero point energies and dipole moments for reactants, products, and transition states (Tables S1–8). See http://www.rsc.org/suppdata/cp/b1/b109970c/

This journal is © The Owner Societies 2002

View Article Online

Published on 16 April 2002. Downloaded by Pennsylvania State University on 17/09/2016 11:27:06.

Computational methods

A. Structures and energies

Ab initio molecular orbital calculations have been carried out on all the molecules involved in this study, using the GAUSSIAN 94,[13a] and GAUSSIAN 98[13b] series of programs. Since electron correlation plays an important role in determining bond energies,[14] the geometries have been optimized at the MP2/6-31G** level with the frozen core approximation[15] for the H-abstraction reactions from DME and MTBE. MP2/6-31G**//MP2/6-31G**, PMP2/6-31G**//MP2/6-31G**, MP4/6-311G(3df,2p)//MP2/6-31G**, PMP4/6-311G(3df,2p)//MP2/6-31G** and CCSD(T)/6-311++G**//MP2/6-31G** levels have been used to evaluate the energetics and kinetics for the H-abstraction reactions from DME whereas the kinetics related to MTBE have been calculated at the MP2/6-31G**//MP2/6-31G** and PMP2/6-31G**//MP2/6-31G** levels. Geometry optimization was followed by vibrational frequency analysis to verify the minimum or transition state character of the compounds.

B. Rate constants and tunneling corrections

The rate constant for the reactions was calculated using the transition state theory.[16] The second-order rate constant in units of cm^3 $molecule^{-1}$ s^{-1} is formulated as

$$k(T) = \frac{k_B T}{h} \frac{q_{TS}}{q_{RH} q_{OH}} \exp\left(-E_c^{forw}/k_B T\right) \quad (1)$$

where k_B is Boltzmann's constant, T is the temperature, h is Planck's constant, the q are the molecular partition functions for the reactants (RH and $^{\bullet}$OH) and the transition state, E_c^{forw} is the forward potential energy barrier that includes the zero-point energy (ZPE) correction indicated by the subscript c.

The tunneling correction was performed by following the procedure of Eckart's unsymmetric barrier method. The Eckart potential energy barrier goes through the zero-point-corrected energies at the reactants, transition states, and products.[17] The Eckart potential function is described by Truong and Truhlar[18] as

$$V = -\frac{ay}{1-y} - \frac{by}{(1-y)^2} \quad (2)$$

where

$$y = -e^{\lambda x} \quad (3)$$

and λ is the range parameter and x the reaction coordinate.

Solving the Schrödinger equation with the Eckart potential function gives the transmission probability, $k(E)$, and the rate constant that includes tunneling can be shown as

$$k_{tunn}(T) = \frac{1}{h} \frac{q_{TS}}{q_{RH} q_{OH}} \int_0^\infty e^{-E/kT} \kappa(E)\, dE \quad (4)$$

The tunneling correction, Γ^*, can be defined as the ratio between $k_{tunn}(T)$ and the classical rate constants calculated by integrating transmission probabilities over all possible energies.

$$\Gamma^*(T) = \exp\left(E_c^f/kT\right) \int_0^\infty \exp(-E/kT)\kappa(E)\, dE \quad (5)$$

The superscript f indicates that this is the barrier for the forward reaction. The barriers that include zero-point corrections are represented with a subscript c, whereas the subscript u is used for the barriers that do not include the zero-point corrections.

As already mentioned by Osman *et al.*[19] the treatment of the complexity of the system of pathways was simplified by the assumption that once a specific pathway has started, it will proceed to completion independent of other pathways. On the basis of this assumption, the rate constant for the abstraction of hydrogen has been considered as the average of the rate constants for the individual processes weighted by the Boltzmann factors of the transition states. The total rate constant of $^{\bullet}$OH disappearance is the sum of these individual rate constants.

Results and discussion

A. The reaction between dimethyl ether and $^{\bullet}$OH

Reactants. The optimized equilibrium conformer for CH_3OCH3 (**1a**) has C_{2v} symmetry with two equivalent CO bonds and two distinct hydrogen environments and is in line with experimental results[20](Fig. 1). The two in-plane hydrogens (H1 and H4) are *trans* with respect to the CO bonds with bond lengths of 1.086 Å, eclipsing the oxygen atom ("eclipsed, eclipsed", **EE** conformer). The internal rotation is defined as the rotation of the methyl groups from the ("eclipsed, eclipsed", **EE**) equilibrium position.[21] The rotation of a single methyl group with a barrier of 2.52 kcal mol^{-1} (with ZPE) yields the **SE** confomer (**1b**) possessing C_s symmetry ("staggered, eclipsed", **SE**). The **SS** (**1c**) conformer is reached by the simultaneous rotation of both methyl groups by 180°, pre-

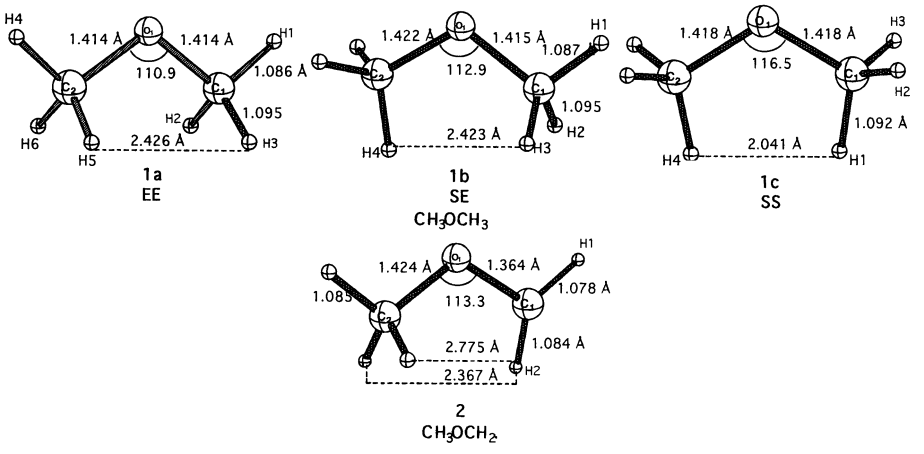

Fig. 1 MP2/6-31G** optimized geometries for dimethyl ether equilibrium (**1a**), lower barrier (**1b**), upper barrier (**1c**) rotational conformers and methoxy methyl radical, $CH_3OCH_2^{\bullet}$ (**2**).

View Article Online

Published on 16 April 2002. Downloaded by Pennsylvania State University on 17/09/2016 11:27:06.

serving the equilibrium C_{2v} symmetry ("staggered, staggered", **SS** conformer). The response to this steric repulsion between the methyl groups is a widening of the C1OC2 angle to 116.5°. The large barrier has been attributed to the reorganization of the lone pair orbital.[21] The source of the reorganization is the 5° opening of the C1OC2 angle, causing the lone pair p character to increase from $sp^{1.5}$ to $sp^{1.7}$ on reaching the top of the barrier.[21]

In the **EE** conformer the C1H2, C1H3, C2H5 and C2H6 bonds are antiperiplanar to the lone pairs on the oxygen. These CH bonds are longer and weaker than the C–H_{gauche} bonds (C1H1 and C2H4) as expected due to the Perlin effect. The existence of the Perlin effect[22–24] in nuclear magnetic resonance spectra has been previously explained by quantitative perturbational molecular orbital (PMO) theory[25] in terms of the effects of lone pairs upon the lengths, strengths and, therefore, the chemical reactivities of vicinal C–H bonds.[22] This effect has been interpreted as the result of $n_O \rightarrow \sigma^*_{C-H}$ hyperconjugation in the language employed by Cieplak[26a] or as a double bond–no bond resonance.[26b] The calculated bond length for the in-plane hydrogen (C1H1 and C2H4) is 1.086 Å, whereas it is 1.095 Å for the out-of-plane CH bond.

Due to the antiperiplanarity of the out of plane CH bond with respect to one of the lone pairs on the oxygen atom, the lengthening of these bonds is associated with a shortening of the CO bond as in the case of the anomeric effect.[27] In the **SE** conformer, the C1O bond (1.415 Å) is shorter than the C2O bond (1.422 Å). This effect is not observed for the other methyl group due to the stereochemistry of the hydrogens with respect to the lone pairs of the oxygen atom. Both **SE** and **SS** have an imaginary frequency, confirming their nature as rotational saddle points. The barrier heights have already been calculated for both single methyl group rotation (2.81 kcal mol^{-1}) and synchronous rotation of both methyl groups (5.06 kcal mol^{-1}) at the MP2/6-31G** level.[21] The results are in good agreement with this study where these barriers are 2.52 and 4.50 kcal mol^{-1}, respectively. On the other hand, the barrier for the single methyl rotation was reported to be 2.78 kcal mol^{-1}, at the MP4(SDQ)/6-31G*//HF/6-31G* level,[28] 2.88 kcal mol^{-1}, at the MP2/6-31G*//HF/6-31G* level with ZPE,[28] and 2.72 kcal mol^{-1}, from microwave spectroscopy[29] (Table 1).

Transition structures and products. Based on the bond strength, the hydrogens in DME can be classified into two categories represented as diastereotopic methyl hydrogens. The hydrogen abstraction by $^{\bullet}$OH proceeds preferentially from the longer CH bonds: C1H2, C1H3, C2H5 and C2H6, resulting in the formation of **TS1-2a** or **TS1-2b**. H-abstraction from the shorter bonds (C1H1 and C2H4) leads to the formation of **TS1-2c**.

The long-range attractive interactions between the H of the $^{\bullet}$OH and the lone pairs of the O of the ether play a role in stabilizing the transition structures. **TS1-2a** and **TS1-2c** have stronger dipolar interactions between the OH bonds and the lone pairs on O1 and are lower in energy than **TS1-2b**. The strength of the long range stabilizing interaction between the hydroxyl group and the lone pairs of the oxygen of the ether group can be estimated to be 1 kcal mol^{-1} by comparing structures **TS1-2a** and **TS1-2b** at the MP2/6-31G** level.

In the transition state, **TS1-2a**, the CO bond length from which hydrogen abstraction occurs decreases by 0.015 Å whereas the other CO bond increases by 0.012 Å. **TS1-2a** is an early transition state, whereas **TS1-2c** is a late transition state. The elongation of the C1H2 bond in **TS1-2a** is 0.089 Å only, whereas in **TS1-2c** it is elongated by 0.123 Å. The C1–O2 distance in the transition states is inversely proportional to the barrier; the smaller the barrier, the longer is the C1–O2 distance. Note that the HOH2 angle is 94.9° in **TS1-2a** and is close to a right angle indicating that a perpendicular approach of $^{\bullet}$OH is preferred.

The reaction of DME (**1a**) with $^{\bullet}$OH *via* **TS1-2a** has a barrier of 3.62 kcal mol^{-1}, and 1.43 kcal mol^{-1} (with ZPE), whereas **TS1-2c** is a late transition state with a barrier of 5.23 kcal mol^{-1}, 4.13 kcal mol^{-1} and 4.41 kcal mol^{-1} (with ZPE) at the PMP2/6-31G**, MP4/6-311G(3df,2p) and CCSD(T)/6-311++G** levels, respectively (Table 1). The H-abstraction reaction from DME is exothermic by 18.66 kcal mol^{-1} and 19.48 kcal mol^{-1} at the PMP2/6-31G** and PMP4/6-311G(3df,2p) levels. These observations are consistent with Hammond's postulate confirming the fact that **TS1-2a** is earlier than **TS1-2c**. Also the distance of approach of $^{\bullet}$OH to **TS1-2a** is 1.366 Å as compared to 1.278 Å in **TS1-2c**.

A prereactive complex (**Complex1-2**) between the OH radical and DME has been located. In this complex, the hydrogen atom of the OH radical points towards the oxygen even though the OH group has to flip over in order to abstract the hydrogen (Fig. 2). This complex lies 8.00 kcal mol^{-1} lower in energy than the separated reactants and increases the initial barrier (6.57 kcal mol^{-1} with MP2/6-31G**) to more than twice its initial value. The experimental barrier[30] being only 0.39 kcal mol^{-1} we have used the separated reactants to evaluate the kinetics of DME as in the case of hydrogen abstraction from propanol and methanol.

In the methoxymethyl radical (**2**), the CO bond on the methylene side is shortened from 1.414 Å in **1a** to 1.364 Å, due to the electron flow from the radical towards the CO bond. (Fig. 1).

B. The reaction between methyl *tert*-butyl ether and $^{\bullet}$OH

Reactants. The molecular structure of MTBE (Fig. 3) at the MP2/6-31G** level gives reasonable agreement with the parameters derived from electron diffraction studies.[20b] The presence of the *tert*-butyl group alters the geometrical parameters of DME. The C2O1 bond is 1.441 Å in MTBE (**3a**) in comparison to 1.414 Å in DME (**1**) mainly due to the electron donor character of the *tert*-butyl group. The C1H1 and C1H2 bonds are antiperiplanar to the lone pairs of the ether oxygen and are longer than the C1H3 bond due to the Perlin effect.[22] As explained earlier, the out-of-plane CH bonds are weaker as a result of an $n_O \rightarrow \sigma^*_{C-H}$ interaction between a

Table 1 Barrier heights for synchronous or single methyl rotations in dimethyl ether and methyl *tert*-butyl ether (kcal mol^{-1})[a]

	6-31G**[b]	6-31G(d,p)[c]	6-31G*[d]	6-311G(3df,2p)[e]	Exp.
Dimethyl ether					
(**1a**) EE → (**1b**) SE	2.52	2.81	2.88		2.72[f]
(**1a**) EE → (**1c**) SS	4.50	5.06		4.72	
Methyl *tert*-butyl ether					
3a → **3b**	3.29		3.25		3.57[g]

[a] MP2 energies are calculated with the inclusion of ZPE. [b] This work. [c] Ref. 21. [d] Ref. 28. [e] Ref. 31 [f] Ref. 29. [g] Ref. 32.

View Article Online

Published on 16 April 2002. Downloaded by Pennsylvania State University on 17/09/2016 11:27:06.

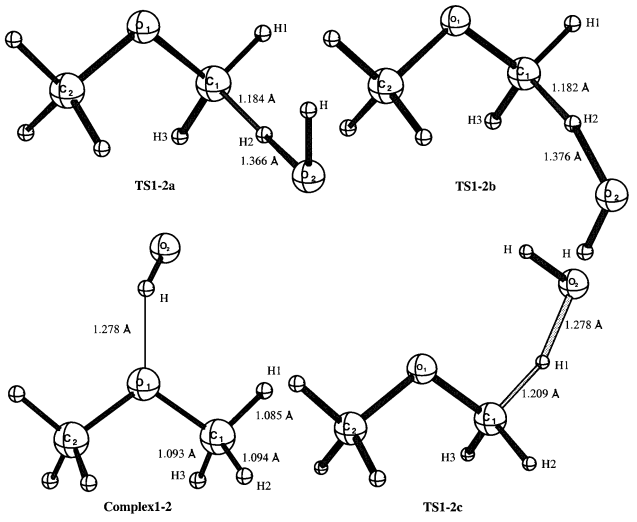

Fig. 2 MP2/6-31G** optimized geometries for three transition states and the complex for H-abstraction from DME.

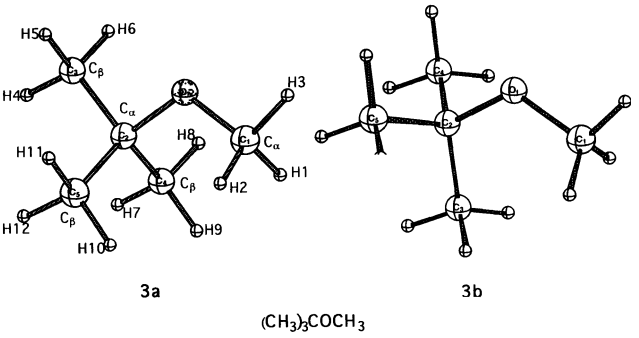

Fig. 3 MP2/6-31G** optimized geometries for methyl *tert*-butyl ether (**3a**) and its rotational conformer (**3b**).

pair of nonbonded electrons on oxygen and the antiperiplanar adjacent CH bond; the double bond–no bond resonance weakens the C1H2 and C2H3 bonds. The internal rotation of a single methyl group around the C2O bond of MTBE (**3a**) by 180° results in a rotational transition structure (**3b**) with an imaginary frequency and preserves the C_s symmetry. The internal rotational barrier which is calculated to be 3.29 kcal mol^{-1} (with ZPE) at the MP2/6-31G** level is in good agreement

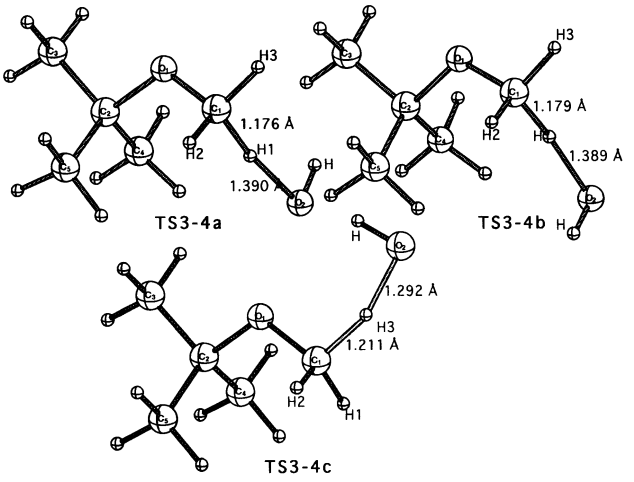

Fig. 4 MP2/6-31G** optimized geometries for the transition states for H-abstraction from methoxy group (C1) of MTBE.

with the 3.57 kcal mol^{-1} found from the analysis of far-infrared spectra in the gas phase.[32]

Transition structures and products. There are three different channels leading to the hydrogen abstraction from MTBE (**3a**): the methoxy group (**TS3-4a**, **TS3-4b**, **TS3-4c**) and the two non-equivalent methyl groups of the *tert*-butyl moiety (**TS3-5a**, **TS3-5b**, **TS3-5c** and **TS3-6a**, **TS3-6b**) can be abstracted by the •OH radical (Figs. 4, 5 and 6).

There are two transition structures, **TS3-4a** and **TS3-4b**, for H-abstraction from the out-of-plane hydrogen of the methoxy group of MTBE due to the orientation of •OH, and one transition structure, **TS3-4c** for H-abstraction from the in-plane hydrogen (Fig. 4). **TS3-4a** is only 0.1 kcal mol^{-1} more stable than **TS3-4b** and is earlier than **TS3-4b** with a shorter CH bond length of 1.176 Å and an OH bond of 1.390 Å. The hydroxyl radical abstracts a hydrogen (H1) in a gauche orientation with respect to the plane formed by the atoms C2O1C3 in MTBE. As mentioned earlier, due to the Perlin effect C1H1 is longer and weaker than its homologues C1H2 and C1H3. Thus, H1 will be preferentially abstracted over the others in **TS3-4a**.

In **TS3-4c** there is a strong dipolar interaction between the H of •OH and O1 (2.439 Å). Nevertheless, the calculated barrier height is 1.64 and 1.14 kcal mol^{-1} higher than the one for **TS3-4a** at the MP2 and PMP2 levels, respectively, due to the fact

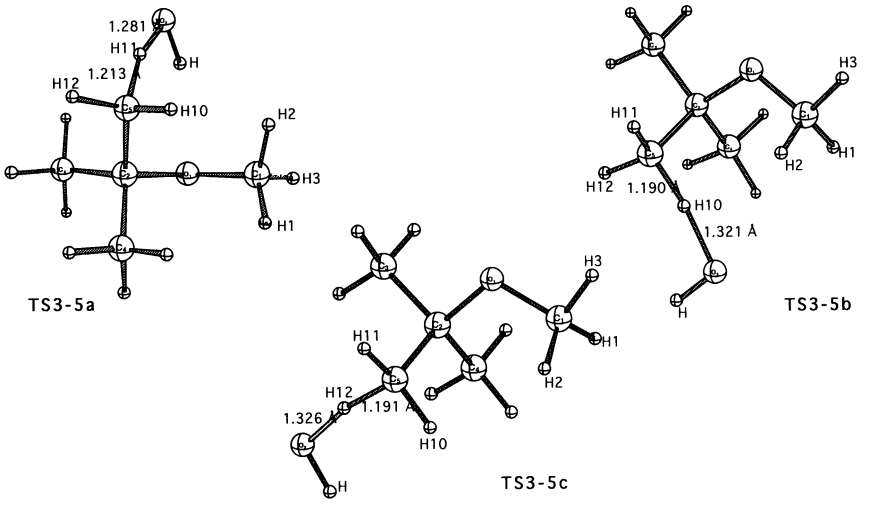

Fig. 5 MP2/6-31G** optimized geometries for the transition states for H-abstraction from the *tert*-butyl (C5) group of MTBE.

View Article Online

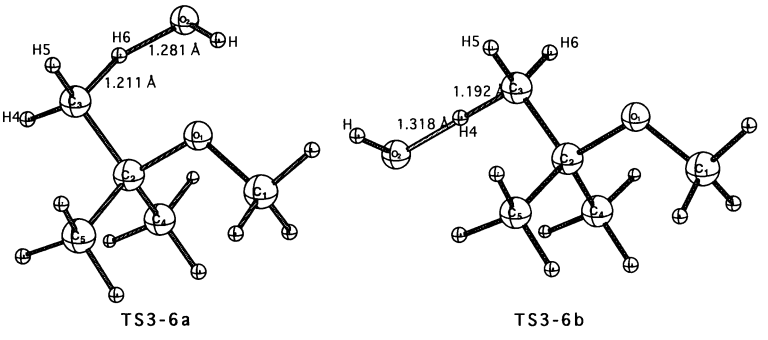

Fig. 6 MP2/6-31G** optimized geometries for the transition states for H-abstraction from the *tert*-butyl (C3) group of MTBE.

Published on 16 April 2002. Downloaded by Pennsylvania State University on 17/09/2016 11:27:06.

that the CH bond for the in-plane hydrogen is stronger and shorter than the out-of-plane hydrogen. On the other hand, the early transition state, **TS3-4a** has shorter breaking CH bond (1.176 Å) and a longer C1–O2 distance (2.560 Å) than the latter transition state structure, **TS3-4c**, where these distances are 1.211 Å and 2.396 Å, respectively. The C1–O2 distance in the transition states is inversely proportional to the barrier; the smaller the barrier, the longer is the C1–O2 distance. These observations are consistent with Hammond's postulate confirming the fact that **TS3-4a** is earlier than **TS3-4c**. Thus, H-abstraction is favored for the out-of-plane hydrogens.

In **TS3-5a**, **TS3-5b**, and **TS3-5c** $^{\bullet}$OH abstracts the hydrogen from the out-of-plane methyl group. According to Hammond's postulate the smaller barrier correlates with the shorter breaking CH bond and the longer the C1–O2 distance in the transition state. Although **TS3-5b** and **TS3-5c** have shorter breaking CH bonds (1.190 Å) and (1.191 Å) and longer C5–O2 distances (2.503 Å) and (2.500 Å), respectively, than **TS3-5a** where the breaking CH bond is 1.213 Å and the C5–O2 distance 2.226 Å, **TS3-5b** and **TS3-5c** are 2.24 kcal mol^{-1} and 2.66 kcal mol^{-1}, respectively, higher in energy than **TS3-5a**. This is due to the presence of stabilizing dipolar interactions between the H of $^{\bullet}$OH and O1 (2.075 Å) in **TS3-5a**.

When $^{\bullet}$OH abstracts the hydrogen from the in-plane β-carbon (C3) it forms two transition state structures, **TS3-6a** and **TS3-6b**. **TS3-6a** is an early transition structure because of the presence of stabilizing dipolar interactions between the H of $^{\bullet}$OH and O1 (2.104 Å). The calculated barrier height for **TS3-6a** is 2.38 and 2.51 kcal mol^{-1} lower than that of **TS3-6b** at MP2 and PMP2 levels, respectively.

There is a correlation between the barrier height and the distance between the oxygen of $^{\bullet}$OH and the carbon from which hydrogen is abstracted.[33] Early transition states occur at shorter C–H bonds and longer CO distances. The transition state for **TS3-4a** occurs at the earliest point along the reaction coordinate since it has the shortest CH breaking bond, but the barrier height (3.24 kcal mol^{-1} at PMP2/6–31G** level) is higher than the ones for **TS3-5a**, **TS3-5b**, and **TS3-6a** because of the absence of intramolecular hydrogen bonds. Hammond's postulate does not hold in these cases, because the reaction coordinates are not comparable.

The C_α radical is formed by hydrogen abstraction from the methoxy side of MTBE. The C1O bond is shorter in **4** (1.366 Å) than in **3a** (1.418 Å). On the other hand, the C2O bond in **4** is slightly longer (1.452 Å) than in **3a** (1.441 Å). This behavior can be attributed to an electron flow from the lone pairs of the oxygen towards the radical on C_α(Fig. 7). The C_β radicals are formed as a result of H-abstraction from the in-plane (C3) and out-of-plane (C4 or C5) carbon atoms of the *tert*-butyl group. As in the case of hydrogen abstraction from C_α, the CC bond vicinal to C_β from which hydrogen has been abstracted shortens (1.494 Å, 1.497 Å) as compared to its initial length in **3a** (1.522 Å, 1.527 Å). The C_βC shortening in radicals **5** and **6** is not as drastic as the C_αO shortening in radical **4**. As a matter of fact, compound **4** is 6.30 kcal mol^{-1} (6.83 kcal mol^{-1} with ZPE) and 8.42 kcal mol^{-1} (7.61 kcal mol^{-1} with ZPE) more stable than **5** and **6** at PMP2/6-31G** level, respectively. The radicals have similar geometrical parameters as the transition structures, the C1O and C2O bonds for the radicals **4**, **5** and **6** are slightly shorter than the corresponding values in the transition structures.

C. Kinetics of H-abstraction

The forward and reverse corrected energy barriers have been used to calculate the rate constants. The zero curvature approximation of tunneling corrections (ZCG) to the rate constants has also been applied. The rate constants measured from earlier experimental work on the kinetics of the H-abstraction from dimethyl ether (DME) and methyl *tert*-butyl ether are shown in Tables 2 and 3.[1,34–45] The calculated rate constants including ZPE with quantum tunneling at room temperature for H-abstraction reactions from DME and MTBE are shown in the Tables 4 and 5 together with the experimental values. In the literature,[18] for reactions where hydrogen transfer takes

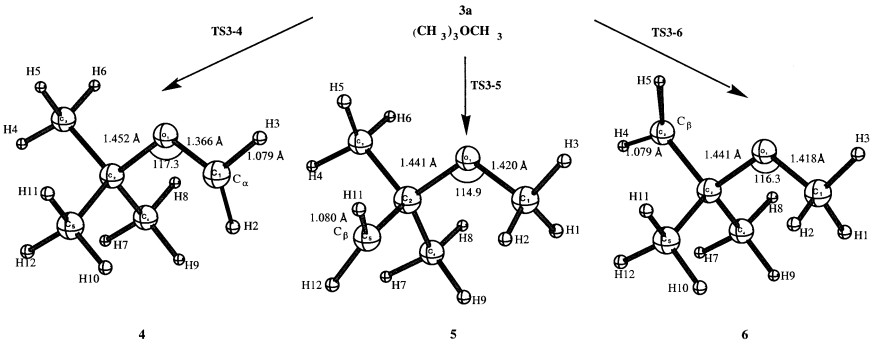

Fig. 7 MP2/6-31G** optimized geometries for the radicals **4**, **5** and **6** formed after the H-abstraction from MTBE.

View Article Online

Published on 16 April 2002. Downloaded by Pennsylvania State University on 17/09/2016 11:27:06.

Table 2 Summary of experimental rate measurements for CH_3OCH_3 + $^{\bullet}OH$ reaction at 298 K

	10^{12} k/cm^3 molecule^{-1} s^{-1}
Mallard *et al.* (1984)[34]	2.46
Tully and Droege (1987)[35a]	2.95
Wallington *et al.* (1988)[36b]	2.49
Wallington *et al.* (1989)[37c]	2.32
Nelson *et al.* (1990)[38d]	2.35
Mellouki *et al.* (1995)[1a]	2.82
Arif *et al.* (1997)[39a]	2.95
DeMore and Bayes (1999)[30e]	2.86
Atkinson (1999)[40]	2.90
This work	
MP2/6-31G**	0.405
PMP2/6-31G**	0.470
MP4(SDTQ)/6-311G(3df,2p)//MP2/6-31G**	1.000
PMP4(SDTQ)/6-311G(3df,2p)//MP2/6-31G**	0.787
CCSD(T)/6-311++G**	0.736

[a] LP-LIF, laser photolysis-laser induced fluorescence. [b] FP-RF, flash photolysis-resonance fluorescence. [c] RR, relative rate. [d] PR-KS, pulse radiolysis-kinetic spectroscopy. [e] Stop-flow.

Table 3 Summary of experimental rate measurements for the $(CH_3)_3COCH_3$ + $^{\bullet}OH$ reaction at 298 K

	10^{13} k/cm^3 molecule^{-1} s^{-1}
Cox and Goldstone(1988)[41a]	2.50
Wallington *et al.* (1988)[42b]	3.09
Wallington *et al.* (1989)[37a]	3.24
Atkinson (1990)[43]	2.83
Japar *et al.* (1990)[44]	2.94
Smith *et al.* (1991)[45a]	2.99
Arif *et al.* (1997)[39c]	2.98
Mitani *et al.* (2002)[45]	2.00
This work[d]	
MP2/6-31G**	0.063
PMP2/6-31G**	0.087

[a] RR, relative rate. [b] FP-RF, flash photolysis-resonance fluorescence. [c] Stop-flow. [d] k_{total} is calculated by summing the calculated rate constants for the H-abstraction from the methoxy group and from the *tert*-butyl group of MTBE.

place, the tunneling effect is taken into account, especially in the reactions with high energy barriers. As expected, the tunneling correction improves the values of the calculated rate constants.

D. The reaction between dimethyl ether and $^{\bullet}OH$

In the reaction between dimethyl ether and hydroxyl radical

$$CH_3OCH_3 + {}^{\bullet}OH \rightarrow CH_3OCH_2{}^{\bullet} + H_2O \qquad (5)$$

there are three potentially abstractable hydrogens for each methyl group. **TS1-2a** and **TS1-2b** refer to the attack of $^{\bullet}OH$ to the out-of-plane hydrogen, **TS1-2c** corresponds to the abstraction of the in-plane hydrogen. **TS1-2a** is energetically 1 kcal mol^{-1} lower than **TS1-2b** at the MP2/6-31G** level. The kinetic calculations are based on the **TS1-2a** for the out-of-plane hydrogen and **TS1-2c** for the in-plane hydrogen abstraction.

In the adiabatic analysis of the B3LYP/6-311++G(d,p) on the vibrational modes of DME carried out by Cremer *et al.*[46] the in-plane CH stretching frequency was found to be 3102 cm^{-1} and the out-of-plane vibrational frequency was 2980 cm^{-1}. Based on the experimental stretching frequencies (2981, 2874) the CH dissociation energies (D_0) have been calculated as 103.8 and 93.7 kcal mol^{-1}, respectively.[47] The difference between the energies of activation for the abstraction of the in-plane hydrogen and the out-of-plane hydrogen is 1.61 kcal mol^{-1} (PMP2/6-31G**), 2.7 kcal mol^{-1} (MP4/6-311G(3df,2p) and 3.00 kcal mol^{-1} (CCDSD(T)/6-311++G**) in line with the CH bond dissociation energies calculated by Cremer *et al.*,[47] indicating that the abstraction of an out-of-plane H atom is easier than of an in-plane H atom.

The bond dissociation energy for the homolytic cleavage of the out-of-plane hydrogen

$$CH_3OCH_3 \rightarrow CH_3OCH_2{}^{\bullet} + H^{\bullet}$$

in this work at 298 K has been calculated as 93.16 kcal mol^{-1}, 92.11 kcal mol^{-1}, 94.40 kcal mol^{-1}, 95.73 kcal mol^{-1}, and 94.40 kcal mol^{-1} at MP2/6-31G**, PMP2/6-31G**, PMP4/6-311G(3df,2p), and CCSD(T)/6-311+G** levels, respectively, while the experimental value is 93.00 kcal mol^{-1}.[48]

The dominant factor that determines the rate constant is the barrier height including the ZPE correction. The experimental activation barrier[30] is 0.98 kcal mol^{-1} and the calculated activation barrier is 1.43 kcal mol^{-1} at the PMP4/6-311G(3df,2p) and CCSD(T)/6-311++G** levels. The imaginary frequency of **TS1-2a** is smaller by about 415 cm^{-1} than the one in **TS1-2c**, indicating that the barrier is wider and thus reducing the effect of tunneling on the rate constant for the former transition structure. It is known that the incomplete inclusion of correlation effects in MP2 overestimates the barrier heights. However, regarding the bond energies it may be that the errors cancel each other because of the ground state nature of the structures involved. Therefore, the calculated bond energies are remarkably in good agreement with the experimental values.

There are four abstractable symmetric out-of-plane hydrogens in DME, the rotational symmetry number (2) due to its C_{2v} symmetry is not introduced in the calculation of partition function, therefore, the calculated rate constant for the H-abstraction from the out-of-plane hydrogen is multiplied by 4. The overall rate constant is evaluated as the sum of the rate constants for H-abstraction from the out-of-plane and the in-plane hydrogens.

$$k_{total} = (4k_{out-of-plane-H}) \times \text{Boltzmann factor} + (2k_{in-plane-H}) \times \text{Boltzmann factor} \qquad (6)$$

The calculated rate constants ($k_{MP2} = 4.05 \times 10^{-13}$ cm^3 molecule^{-1} s^{-1}, $k_{PMP2} = 4.70 \times 10^{-13}$ cm^3 molecule^{-1} s^{-1}, $k_{MP4} = 1.00 \times 10^{-12}$ cm^3 molecule^{-1} s^{-1}, $k_{PMP4} = 7.80 \times 10^{-13}$ cm^3 molecule^{-1} s^{-1}, and $k_{CCSD(T)} = 7.35 \times 10^{-13}$ cm^3 molecule^{-1} s^{-1}) are almost 7, 6, 3, 3.7 and 4 times lower, respectively, than the experimental rate constant[39] ($k_{exp} = 2.90 \times 10^{-12}$ cm^3 molecule^{-1} s^{-1}) at 25 °C. The MP4, PMP4 and CCSD(T) results agree well with the experimental values.

The Boltzmann factors for the two types of transition structures are highly different. The contribution of the lower barrier transition structure, **TS1-2a**, is greater (0.977) than that of the higher barrier transition structure, **TS1-2c** (0.023) at MP2/6-31G** level. The same trend is observed with the PMP2 energetics (0.938 and 0.062, respectively), and the CCSD(T)/6-311+G** energetics (0.990 and 0.010, respectively). The tunneling corrections with CCSD(T)/6-311++G** using the MP2 optimized geometry, is reasonable for **TS1-2a**, but mean-

View Article Online

Published on 16 April 2002. Downloaded by Pennsylvania State University on 17/09/2016 11:27:06.

Table 4 Kinetic parameters[a] for DME calculated at the MP2/6-31G** optimized geometries, PMP2/6-31G**, MP4(SDTQ)/6-311G(3df,2p), PMP4(SDTQ)/6-311G(3df,2p) and CCSD(T)/6-311++G** levels

	TS1-2a (out-of-plane H)					**TS1-2c** (in-plane H)				
	MP2	PMP2	MP4	PMP4	CCSD(T)	MP2	PMP2	MP4	PMP4	CCSD(T)
Barriers/kcal mol^{-1}										
E_u (forward)	6.58	4.78	2.55	1.35	2.55	9.28	6.98	5.89	4.49	5.91
E_u (reverse)	24.42	22.58	7.85	20.48	21.72	27.13	24.92	11.18	23.62	25.43
E_c (forward)	5.45	3.62	1.43	0.22	1.43	7.53	5.23	4.13	2.73	4.42
E_c (reverse)	23.93	22.28	7.35	19.98	21.22	26.00	23.80	10.05	22.49	23.86
Imaginary frequencies/cm^{-1}	1703.7					2119.0				
Tunneling corrections (τ*)	2.38×10^3	153	6.48	0.67	4.82	64.24×10^3	1.99×10^3	4.74×10^2	38.50	5.56×10^2
Rate constants/cm^3 molecule^{-1} s^{-1} [b]										
$10^{13}k$ (calc)[c]	4.08	5.76	10.03	7.88	7.38	3.20	4.82	7.78	6.52	5.39
Boltzmann factor	0.977	0.938	0.990	0.990	0.990	0.023	0.062	0.010	0.010	0.010
$10^{13}k$[d]	3.98	4.40	9.92	7.80	7.31	0.074	0.300	0.078	0.065	0.054
$10^{13}k_{total}$[e] (calc)	4.05	4.70	10.00	7.87	7.36					

[a] ZPE correction is included. [b] $T = 298.15$ K. [c] Tunneling correction is included. [d] k is calculated by the multiplication of k_i in section C by Boltzmann factor. [e] k_{total} for the H-abstraction from DME is calculated by the sum of the rate constants calculated for each channel at each level.

ingless for **TS1-2c**, due to the high imaginary frequency and the activation barrier.

E. The reaction between methyl *tert*-butyl ether and $^{\bullet}$OH radical

The reaction of $^{\bullet}$OH with methyl *tert*-butyl ether occurs *via* three different channels. **TS3-4a** and **TS3-4b** correspond to the H-abstraction from the out-of-plane hydrogen of the methoxy group of MTBE. **TS3-4c** is the transition for the hydrogen abstraction from in-plane hydrogen of methoxy group of MTBE. **TS3-5a**, **TS3-5b**, **TS3-5c**, **TS3-6a**, and **TS3-6b** refer to the transition structures for H-abstraction from the *tert*-butyl group. The overall rate constant for the H-abstraction from the methoxy group of MTBE is evaluated as the sum of the rate constants for H-abstraction from the out-of-plane and the in-plane hydrogens.

$$k_{methoxy} = (2k_{out-of-plane-H}) \times \text{Boltzmann factor} + (k_{in-plane-H}) \times \text{Boltzmann factor} \quad (7)$$

Similarly, the total rate constant is also calculated for the *tert*-butyl group by taking into consideration the Boltzmann factors for each channel.

The ratio of the rate constants calculated at the MP2/6-31G** level predicts 58% hydrogen abstraction from the methoxy group as compared to the *tert*-butyl group. This ratio is in agreement with the experimental results of Arif *et al.*[39] and Tuazon *et al.*[49] This behavior is also reproduced with PMP2 energies, where the contribution to the rate constant from methoxy group is to 63%. The CH bond strengths at MP2/6-31G** level for the methoxy and *tert*-butyl group have been calculated as 93.16 kcal mol^{-1} and 99.60 kcal mol. These values at PMP2/6-31G** level are 92.11 kcal mol^{-1} and 97.78 kcal mol^{-1}, whereas the experimental values[50] are 93.30 and 98.12 kcal mol^{-1}, respectively.

As in the case of DME, the difference between the energies of activation for the abstraction of the in-plane hydrogen and the out-of-plane hydrogen of the methoxy group is 1.65 kcal mol^{-1} (MP2/6-31G**) and 1.14 kcal mol^{-1} (PMP2/6-31G**), indicating that the abstraction of an out-of-plane H atom should be easier than of an in-plane H atom. The calculated rate constants at MP2/6-31G** level shows that the H-abstraction from the in-plane hydrogen (1.82×10^{-14} cm^3 molecule^{-1} s^{-1}) is much slower than the H-abstraction from the out-of-plane hydrogen (1.11×10^{-17} cm^3 molecule^{-1} s^{-1}) of the methoxy group of MTBE. At the PMP2/6-31G** level, these values are 2.42×10^{-14} and 7.38×10^{-15} cm^3 molecule^{-1} s^{-1} for the H-abstraction from the in-plane hydrogen and out-of-plane hydrogen, respectively. Both methods have reproduced the expected relationship between the CH bond strengths and the reaction kinetics.

On the other hand, the experimental rate constants for reactions (i) and (ii) at 298 K are 8.8×10^{-13} and 5.6×10^{-13} cm^3 molecule^{-1} s^{-1}.[49]

$$(CH_3)_3COCH_3 + {}^{\bullet}OH \rightarrow (CH_3)_3COCH_2{}^{\bullet} + H_2O \quad \text{(i)}$$

$$(CH_3)_3COCH_3 + {}^{\bullet}OH \rightarrow CH_3OC(CH_3)CH_2{}^{\bullet} + H_2O \quad \text{(ii)}$$

Although in qualitative agreement with the experimental values, the calculated rate constants 5.58×10^{-14} cm^3 molecule^{-1} s^{-1} and 3.16×10^{-14} cm^3 molecule^{-1} s^{-1} at PMP2/6-31G** are almost 10 times lower than the experimental values.

Recently, the hydrogen abstraction from aldehydes by $^{\bullet}$OH investigated by Vivier-Bunge *et al.*[51] has produced PMP2 effective activation energies overestimated by about 3 kcal mol^{-1}. CCSD(T) was found to be the most appropriate method to use to obtain adequate activation energies. An overestimation of the activation energies by MP2 for the hydrogen abstraction from methane and fluorinated methane has also been mentioned by Jursic.[52] Similarly, Sekusak *et al.*[53] have used MP2/6-31G** to calculate the optimized geometries, harmonic vibrational frequencies to model the reactivity of fluoroethane with hydroxyl radical. However, accurate energies have been calculated using the G2 theory. Boyd *et al.*[54] have followed the hydrogen abstraction from ethane by the hydroxyl radical by using MP2/6-31G**, energies were calculated using a modified version of Gaussian-2 theory. These recent investigations on similar reactions together with the results of this work suggest the usage of MP2 for geometry optimization rather than for the energetics of the process.

Direct dynamic calculations including variational transition state calculations have been carried out to model the hydrogen abstraction from NH_3, HBr and CH_2F_2.[55] We have checked the validity of the TST approach at the vicinity of the transition state by fully optimizing several structures on the IRC of DME. These calculations have confirmed the coincidence of the transition state with the saddle point.

Another source of error in the kinetics of the reactions studied is the zero-curvature approximation for the calculation of

Published on 16 April 2002. Downloaded by Pennsylvania State University on 17/09/2016 11:27:06.

Table 5 Kinetic parameters[a] for methyl *tert*-butyl ether at the MP2/6-31G** optimized geometries and at the PMP2/6-31G** level (in parentheses)

	TS3-4a	TS3-4c	TS3-5a	TS3-5b	TS3-5c	TS3-6a	TS3-6b
Barriers/kcal mol^{-1}							
E_u (forward)	6.09 (4.37)	8.17 (5.93)	5.18 (2.88)	8.09 (6.02)	8.49 (6.38)	5.24 (2.94)	8.34 (6.18)
E_u (reverse)	24.98 (23.38)	26.06 (24.95)	17.19 (15.30)	20.10 (18.34)	20.50 (18.69)	15.50 (13.53)	18.60 (16.77)
E_c (forward)	4.96 (3.24)	6.61 (4.38)	4.41 (2.12)	6.34 (2.12)	6.89 (4.78)	4.34 (2.04)	6.72 (4.55)
E_c (reverse)	24.42 (22.82)	26.06 (23.95)	17.57 (15.68)	19.58 (15.58)	20.05 (18.24)	15.98 (14.01)	18.35 (16.52)
Imaginary frequencies/cm^{-1}	1528.0	2056.58	2072.5	1755.0	1776.8	2051.6	1754.5
Tunneling corrections $\times 10^{-2}$ (τ*)	10.37 (0.810)	156.9 (5.29)	6.435 (0.166)	108.6 (0.156)	217.3 (9.64)	5.86 (0.150)	170 (7.05)
Rate constants/cm^3 molecule^{-1} s^{-1} [b]							
$10^{14}k$[c]	1.93 (2.78)	1.88×10^{-2} (5.68)	0.94 (1.71)	2.97 (6.64)	1.66 (2.63)	1.61 (2.02)	3.12 (4.98)
Boltzmann factor $\times$ 10	9.40 (8.70)	0.60 (1.30)	4.49 (3.15)	0.17 (3.15)	0.068 (0.035)	5.51 (3.60)	0.009 (0.005)
$10^{15}k$[d]	18.2 (24.2)	0.011 (7.38)	4.42 (5.39)	0.51 (0.93)	0.11 (2.09)	8.26 (7.29)	0.28 (0.26)
$10^{14}k_{total}$	3.64 (5.58)[e]				2.64 (3.16)[f]		
$10^{13}k$ (exp)	8.8[g]				5.6[h]		

[a] ZPE correction is included. [b] $T = 298.15$ K. [c] Tunneling correction is included. [d] k is calculated by multiplication of k in section C by the Boltzmann factor. [e] k_{total} for the H-abstraction from the methoxy group. k^{total} *for H-abstraction from the tert-butyl group.* [g] Ref. 49 for H-abstraction from the methoxy group. [h] Ref. 50 for H-abstraction from *tert*-butyl group.

View Article Online

View Article Online

the tunneling correction, since the reaction path allows tunneling in one dimension. More elaborate tunneling calculations, which take into account the local curvature in the vicinity of the TS, would yield larger rate constants. The fact that rigid rotor approximation was used for the calculation of the vibrational partition function may have underestimated the rate constants. A free rotor representation of the low frequency vibration is expected to increase the rate constant.[32]

F. Dipole moments

The dipole moments of DME (1.60 D) and of MTBE (1.45 D) reveal the fact that both ethers are almost equally soluble in a polar solvent in spite of the presence of the *tert*-butyl group. Regarding the transition structures for reaction (1), **TS1-2c** is more polar than **TS1-2a** and the expectation is that **TS1-2c** will contribute in the hydrogen abstraction from DME in a polar environment more than it does in the gas phase. It is expected that the in-plane hydrogens will also be abstracted in solution.

As to the the fate of the hydrogens of the MTBE in polar environment, one can invoke the more polar nature of the transition structures related to hydrogen abstraction from the *tert*-butyl group as compared to the ones for hydrogen abstraction from the methyl group. As shown earlier and in line with experiment, in the gas phase hydrogen abstraction from the methyl group of MTBE proceeds faster than hydrogen abstraction from the *tert*-butyl group. However, in a polar environment the contribution from the *tert*-butyl group is expected to increase.

Conclusion

Ab initio calculations at MP2 and at spin-projected second-order Møller-Plesset (PMP2//UMP2) level of theory with 6-31G** basis set were performed for the $CH_3OCH_3 + OH^{\bullet}$ and $(CH_3)_3COCH_3 + OH^{\bullet}$ reaction systems. The correlation energy corrections was introduced with the coupled cluster method at the CCSD(T)/6-311+G** level and Møller-Plesset (MP4(SDTQ)//MP2/6-311G(3df,2p)) perturbation level in the space of single, double, and quadruple excitations level only for the H-abstraction reaction from DME. The MP4((SDTQ)//MP2)/6-311G(3df,2p))//MP2/6-31G** level provides a more consistent improvement for the forward and reverse reactions, resulting in better agreement between the calculated and the experimental rate constants. Geometric features of the reactants located with MP2/6-31G** level have been in line with the experimental findings.

The barriers for the different transition structures for a given channel have been rationalized by considering the strengths of the breaking bond as well as the orientation of the hydroxyl group with respect to the ether. Bond energies for the C–H bonds have been reproduced adequately with the methodology used.

The experimental results on MTBE regarding the abundance of the abstraction from the methoxy group of MTBE in comparison to the *tert*-butyl are 58% at MP2/6-31G** level, and 63% with PMP2/6-31G** level.

Although *ab initio* calculations of the characteristic tunneling correction suggest tunneling would be significant in the rate calculations, the experimental data shows that the rate constants calculated in this study reproduce the reported experimental results for the H-abstraction reaction from DME, especially, with higher correlation energy correction, CCSD(T)/6-311+G** and MP4(SDTQ)/6-311G(3df,2p) levels. For MTBE the calculated rate constants are almost 10 times lower than the experimental rate constants. Better results are expected with higher *ab initio* methods, such as CCSD(T)/6-311+G** or MP4(SDTQ)/6-311G(3df,2p).

Acknowledgement

Financial support for the work was supported by DPT (98 K 120900) and Tubitak (TBAG-1684). Special thanks go to Prof. Dr R. Osman (Mount Sinai School of Medicine) for his valuable suggestions and J. R. Bolton (Bolton Photosciences Inc.) for providing information about the experimental data.

References

1 A. Mellouki, S. Teton and G. Le Gras, *Int. J. Chem. Kinet.*, 1995, **27**, 791.
2 J. Sehested, T. Mogelberg, T. J. Wallington, E. W. Kaiser and O. J. Nielsen, *J. Phys. Chem.*, 1996, **100**, 17218.
3 A. G. Good and J. S. Francisco, *J. Phys. Chem. A*, 2000, **104**, 1171.
4 T. J. Wallington, J. M. Andino, L. M. Skewes, W. O. Siegl and S. M. Japar, *Chem. Rev.*, 1993, **93**, 671.
5 L. N. Gregerson, J. S. Siegel and K. K. Baldridge, *J. Phys. Chem.*, 2000, **104**, 11106.
6 S. L. Brown, *Regul. Toxicol. Pharmacol.*, 1997, **25**, 256.
7 J. H. Mennear, *Risk Anal.*, 1997, **17**, 673.
8 Secretary Scientific Advisory Board on Toxic Air Pollutants, *Environ. Health Perspect.*, 1995, **103**, 420.
9 K. Tokuhashi, A. Takahashi, M. Kaise, S. Kondo, A. Sekiya, S. Yamashita and H. Ito, *J. Phys. Chem. A.*, 2000, **104**, 1165.
10 T. Y. Chang, R. H. Hammerle, S. M. Japar and I. T. Salmeen, *Environ. Sci. Technol.*, 1988, **22**, 842.
11 L. N. Gregerson, J. S. Siegel and K. K. Baldridge, *J. Phys. Chem. A.*, 2000, **104**, 11106.
12 A. Bottoni, P. Della-Casa and G. Poggi, *J. Mol. Struct.*, 2001, **542**, 123.
13 (*a*) M. J. Frisch, G. W. Trucks, H. B. Schlegel, P. M. W. Gill, B. G. Johnson, M. A. Robb, J. R. Cheeseman, T. Keith, G. A. Peterson, J. A. Montgomery, K. Raghavachari, M. A. Al-Laham, V. G. Zakrezewski, J. V. Ortiz, J. B. Foresman, J. Cioslowski, A. Nanayakkara, M. Challacombe, C. Y. Peng, P. Y. Ayala, W. Chen, M. W. Wong, J. L. Andres, E. S. Replogle, R. L. Martin, D. J. Fox, J. S. Binkley, D. J. DeFrees, J. Baker, J. P. Stewart, M. Head-Gordon, C. Gonzalez, J. A. Pople, *Gaussian 94*, Revision D.3, Gaussian, Inc., Pittsburgh, PA, 1995; (*b*) M. J. Frisch, G. W. Trucks, H. B. Schlegel, G. E. Scuseria, P. M. W. Gill, B. G. Johnson, M. A. Robb, J. R. Cheeseman, V. G. Zakrezewski, T. Keith, J. A. Montgomery, R. E. Stratmann, J. C. Burant, S. Dapprich, J. M Milliam, A. D. Daniels, K. N. Kudin, M. C. Strain, O. Karkas, J. Tomasi, V. Barone, M. Cossi, R. Cammi, B. Mennucci, C. Pomelli, C. Adamo, S. Clifford, G. Ochterski, G. A. Peterson, P. Y. Ayala, K. Morokuma, D. K. Malick, A. D. Rabuck, K. Raghavachari, M. A. Al-Laham, J. V. Ortiz, J. B. Foresman, J. Cioslowski, G. Liu, A. Liashenko, P. Piskorz, I. Komaromi, R. Gomperts, A. Nanayakkara, M. Challacombe, C. Y. Peng, W. Chen, M. W. Wong, J. L. Andres, E. S. Replogle, R. L. Martin, D. J. Fox, J. S. Binkley, D. J. DeFrees, J. Baker, J. P. Stewart, M. Head-Gordon, C. Gonzalez, J. A. Pople, *Gaussian 98*, Revision A.7; Gaussian, Inc.: Pittsburgh, PA, 1998.
14 M. S. Gordon and D. G. Truhlar, *Int. J. Quantum Chem.*, 1987, **31**, 81.
15 W. J. Hehre, L. Radom, P. v. R. Schleyer and J. A. Pople, *Ab initio Molecular Orbital Theory*, John Wiley, New York, 1986.
16 H. S. Johnston, *Gas-Phase Reaction Rate Theory*; The Ronald Press Co., New York, 1966.
17 C. Eckart, *Phys. Rev.*, 1930, **35**, 1303.
18 T. N. Truong and D. G. Truhlar, *J. Chem. Phys.*, 1990, **93**, 1761.
19 N. Luo, C. D. Kombo and R. Osman, *J. Phys. Chem. A*, 1997, **101**, 926.
20 (*a*) U. Blukis, P. H. Kasai and R. J. Meyers, *J. Chem. Phys.*, 1963, **38**, 2753; (*b*) S. Liedle, H. G. Mack, H. Oberhammer, M. R. Imam and N. L. Allinger, *J. Mol. Struct.*, 1989, **198**, 1.
21 V. Pophristic and L. Goodman, *J. Phys. Chem. A*, 2000, **104**, 3231.
22 A. S. Perlin and B. Casu, *Tetrahedron Lett.*, 1969, 292.
23 S. Wolfe, B. M. Pinto, V. Varma and R. Y. N. Leung, *Can. J. Chem.*, 1990, **68**, 1051.
24 S. Wolfe and C. K. Kim, *Can. J. Chem.*, 1991, **69**, 1408.
25 M. H. Whangbo, H. B. Schelegel and S. Wolfe, *J. Am. Chem. Soc.*, 1977, **99**, 1296.

Published on 16 April 2002. Downloaded by Pennsylvania State University on 17/09/2016 11:27:06.

View Article Online

26 (*a*) A. S. Cieplak, *J. Am. Chem. Soc.*, 1981, **103**, 4540; (*b*) A. S. Cieplak and B. D. Tait, *J. Am. Chem. Soc.*, 1989, **111**, 8447; (*c*) C. Romers, C. Altona, H. R. Buys and E. Havinga, *Top. Stereochem.*, 1969, **4**, 39.
27 (*a*) R. U. Lemieux, *Molecular Rearrangements*, ed. P. de Mayo, Interscience, New York, 1964, p. 709; (*b*) R. Arnaud, *J. Comput. Chem.*, 1994, **15**, 1341.
28 S. Tsuzuki and K. Tanabe, *J. Chem. Soc., Perkin Trans. 2*, 1991, 181.
29 P. H. Kasai and R. J. Meyers, *J. Chem. Phys.*, 1959, **30**, 1096.
30 W. B. DeMore and K. D. Bayes, *J. Phys. Chem. A*, 1999, **103**, 2649.
31 L. Goodman, V. Pophristic and F. Weinhold, *Acc. Chem. Res.*, 1999, **32**, 983.
32 J. R. Durig, S. M. Craven, J. H. Mulligan, C. W. Hawley and J. Bragin, *J. Chem. Phys.*, 1973, **58**, 1281.
33 L. Pardo, J. R. Banfelder and R. Osman, *J. Am. Chem. Soc.*, 1992, **114**, 2382.
34 W. G. Mallard, F. Westlely, J. T. Herron, R. F. Hampson, *NIST Chemical Kinetics Database Ver. 6.0*; NIST Reference Data, NIST, Gaithersburg, MD, 1994.
35 F. P. Tully and A. T. Droege, *Int. J. Chem. Kinet.*, 1987, **19**, 251.
36 T. J. Wallington, R. Liu, P. Dagaut and M. Kurylo, *Int. J. Chem. Kinet.*, 1988, **20**, 541.
37 T. J. Wallington, J. M. Andino, L. M. Skewes, W. O. Siegl and S. M. Japar, *Int. J. Chem. Kinet.*, 1989, **21**, 993.
38 L. Nelson, O. Rattigan, R. Neavyn, H. Sidebottom, J. Treacy and O. J. Nielsen, *Int. J. Chem. Kinet.*, 1990, **22**, 1111.
39 M. Arif, B. Dellinger and P. H. Taylor, *J. Phys. Chem. A*, 1997, **101**, 2436.
40 R. Atkinson, D. L. Baulch, R. A. Cox, R. F. Hampson, Jr., J. A. Kerr, M. J. Rossi and J. Troe, *J. Phys. Chem. Ref. Data*, 1999, **28**, 191–393.
41 R. A. Cox and A. Goldstone, *Proceedings of the 2nd European Symposium on the Physico Chemical Behavior of Atmospheric Pollutants*, Riedel Publishing Co., Dordrecht, Holland, 1982, pp. 112–119.
42 T. J. Wallington, P. Dagaut, R. Liu and M. Kurylo, *J. Environ. Sci. Technol.*, 1988, **22**, 842.
43 R. Atkinson, *J. Phys. Chem. Ref. Data*, 1990, Monograph No.1.
44 S. M. Japar, T. J. Wallington, J. F. O. Richert and J. C. Ball, *Int. J. Chem. Kinet.*, 1990, **22**, 1257.
45 (*a*) D. F. Smith, T. E. Kleindienst, E. E. Hudgens, C. D. McIver and J. J Bufalini, *Int. J. Chem. Kinet.*, 1991, **23**, 907; (*b*) M. M. Mitani, A. A. Keller, C. A. Bunton, R. G. Rinker and O. C. Sandall, *J.Hazard. Mater.*, 2002, **B89**, 197.
46 D. Cremer, J. A. Larsson and E. Kraka, in *Theoretical and Computational Chemistry: Theoretical Organic Chemistry*, ed. C. Parkanyi, Elsevier, Amsterdam, 1998, vol. 5, p. 259.
47 R. Wrobel, W. Sander, E. Kraka and D. Cremer, *J. Phys. Chem. A*, 1999, **103**, 3693.
48 D. F. Mac Millen and D. M. Golden, *Ann. Rev. Phys. Chem.*, 1982, **33**, 493.
49 E. C. Tuazon, W. P. L. Carter, S. M. Aschmann and R. Atkinson, *Int. J. Chem. Kinet.*, 1991, **23**, 1003.
50 S. W. Benson, *Thermochemical Kinetics*, John Wiley: New York, 1976.
51 J. R. Alvarez-Idaboy, N. Mora-Oiez, R. J. Boyd and A. Vivier-Bunge, *J. Am. Chem. Soc.*, 2001, **123**, 2018.
52 B. S. Jursic, *Chem. Phys. Lett.*, 1996, **256**, 603.
53 S. Sekusak, H. Güsten and A. Sabljic, *J. Phys. Chem.*, 1996, **100**, 6212.
54 J. M. Martell, A. K. Mehta, P. D. Pacey and R. J. Boyd, *J. Phys. Chem.*, 1995, **99**, 8661.
55 (*a*) J. Espinosa-Garcia and J. C. Corchado, *J. Chem. Phys.*, 1994, **101**, 8700; (*b*) J. Liu, Z. Li, Z. Dai, X. Huang and C. Sun, *J. Phys. Chem. A*, 2001, **105**, 7707; (*c*) A. Gonzalez-Lafont, J. M. Lluch and J. Espinosa-Garcia, *J. Phys. Chem. A*, 2001, **105**, 10 553.

Published on 16 April 2002. Downloaded by Pennsylvania State University on 17/09/2016 11:27:06.